PHYSICAL REVIEW B VOLUME 62, NUMBER 24 15 DECEMBER 2000-II

Electrostatics of quantum dots in high magnetic fields and single far-infrared photon detection

O. Astafiev and V. Antonov*
CREST, Japan Science and Technology Corporation (JST), Kawaguchi-shi, Saitama 332-0012, Japan

T. Kutsuwa and S. Komiyama
Department of Basic Science, University of Tokyo, Komaba 3-8-1, Meguro-ku, Tokyo 153-8902, Japan

(Received 17 March 2000)

Electron transport through a single electron transistor (SET) is studied with and without illumination of far-infrared (FIR) radiation in high magnetic fields. The SET consists of a GaAs/Al$_x$Ga$_{1-x}$As quantum dot (QD). The transport characteristics obtained without the FIR illumination is well analyzed in terms of capacitance matrix by assuming that the QD in strong magnetic fields is split into isolated conductive regions. When a FIR photon is absorbed by a QD upon cyclotron resonance, an excited electron-hole pair induces a charge polarization within the QD, which switches on or off the SET conductance. The absorption of single-FIR photons is thus detected as individual conductance switches of the SET. Experimental results show that the lifetime of the excited state of a QD (with the internal polarization) is longer than the instrumental time constant, 1 ms, in a magnetic field range of $B=3.4-4.2$ T, in which the lowest orbital Landau levels are completely occupied while the higher Landau level with a small number of electrons is slightly occupied. The wavelength of the FIR-photon detection, being determined by the magnetic field applied to the QD, ranges from 0.2 mm to 0.17 mm.

I. INTRODUCTION

The single-electron transistor[1] (SET), formed by a small conducting island weakly coupled to external electron reservoirs, provides us with a unique device that is extremely sensitive to its electrostatic environment as well as to its electromagnetic environment. Due to the sensitivity to the former, the SET has been successfully used as an electrometer that detects small and local charges.[2]

This unique property of the SET, however, has not been fully explored. It is suggested that extremely weak electromagnetic waves could alter the tunnel rate across tunnel junctions, thereby affecting the SET conductance.[3] Experiments show that weak microwave radiation gives rise to photon-assisted tunneling of electrons across tunnel barriers, thereby causing a distinct and systematic change in the SET conductance.[4] Coherent electromagnetic waves coherently couple electron states in a double quantum dot system, which also leads to a change of the SET conductance.[5] In these effects, however, one absorbed photon of relevant electromagnetic waves contributes only one electron to a current through the device and the potentiality of the SET as a charge sensitive device is not fully exhausted.

Sensitive photodetectors with the SET have been proposed.[6,7] In the proposed schemes, however, photons are converted to charges through one of conventional excitation mechanisms, while the SET is added to be used as a low noise charge detector: Due to the indirect use of the SET the detector performance might be restricted.

We report here single-photon detection in the far-infarred (FIR) spectral region by using a SET formed by a semiconductor quantum dot (QD) at high magnetic fields. In our scheme, a FIR photon is absorbed via cyclotron resonance (CR), creating an electron and a hole in the upper and the lower Landau levels (LL's) inside the QD. The excited electron-hole pair induces a polarization of the QD, which in turn switches on (or off) the conductance resonance of the SET. Since the excited electron-hole pair or the associated polarization is long living (more than the instrumental time constant of 1 ms reaching a value as large as 20 min), one absorbed FIR photon yields a distinct measurable pulse in the current through the QD. In the present scheme, therefore, both the photon-to-charge conversion and the charge detection are carried out within the single QD (or the SET), where one absorbed photon leads to an integrated current (the bias current multiplied by the recombination lifetime of the electron-hole pair) of 10^6–10^{12} electrons. This effect thus demonstrates a unique property of the QD as a single-FIR-photon detector, but on the other hand, the distinguished sensitivity of the SET will make this effect a powerful tool for studying the spectroscopy of single QD's in general. Our present work demonstrates the study of CR in a single QD, which was impossible in the conventional transmission studies that needed an array of a large number of QD's.[8] Cyclotron resonance may not be the unique mechanism that switches the SET conductance. Many other mechanisms of intradot excitation may as well significantly influence the SET conductance through the effect of induced polarization or through an induced change in the tunnel coupling of the QD to external leads. Any of such intradot excitation processes may be utilized as a sensitive tool for studying the spectrum of single QD's.

In previous reports we briefly described the single-FIR-photon detection.[9,10] The main purpose of this paper is to describe detailed experimental features of the effect. The first half of this paper will be devoted to comprehensive discussion of electrostatics of the QD's. The electrostatic nature of QD's at high magnetic fields is by itself an interesting subject, and this is of particular importance for our present work because it is the basis of the intradot charge polarization induced by the CR. This paper is organized as follows. In Sec. II, a theoretical framework treating QD's at high mag-

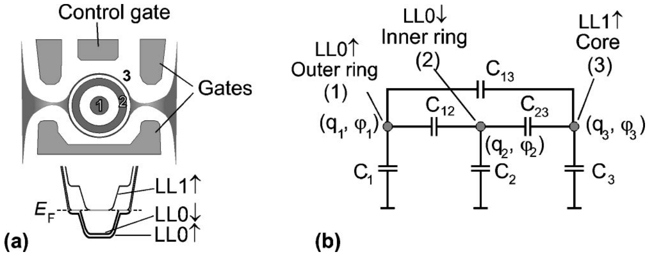

FIG. 1. (a) Schematic top-view of the QD in high magnetic field at $2<\nu<3$. Separated conductive regions, two conductive rings and one core, are formed corresponding to quantized Landau levels. (b) The outer ring (1), the inner ring (2), and the core (3), formed, respectively, by LL0↑, LL0↓, and LL1↑, are capacitively coupled to one another and the surroundings outside.

netic fields is described. Section III is devoted to a description of experimental methods. In Sec. IV A, we describe transport properties of our SET's without FIR illumination to clarify internal structure of the QD's. In Sec. IV B, we present and interpret experimental results obtained by illuminating the QD's with FIR radiation and demonstrate the single-photon detection. Section V is devoted to the discussions of the excited-state lifetime and characteristic features of the present effect when the present SET is viewed as a photon detector.

II. BACKGROUND

Ground states of quantum dots (QD's) in high magnetic fields, B, have attracted considerable attention both theoretically[11–14] and experimentally.[15–17] The studies have been focused in the B range where only the lowest orbital Landau levels (LL's) are occupied. In such a condition,[16,17] especially for relatively small QD's containing less than several tens of electrons in total, the exchange energy term as well as many-body effects are suggested to play an important role. Differently from these works, we focus our attention on relatively large QD's containing a few hundreds of electrons ($N\approx 350$), in which not only the lowest orbital LL's but also the first orbital LL is partially occupied with a small number of electrons (<30), viz., the filling factor of LL's, ν, is larger than or equal to 2. In these relatively large QD's, the exchange term and many-body effects may be of relatively less importance, and a single-particle picture will give a reasonable description provided that self-consistent electrostatic energy is properly considered.[15,18]

Spin-up and spin-down lowest orbital LL's are resolved in the present experiments, where the Zeeman splitting, $g^*\mu B \approx 200\ \mu\text{eV}$ at $B=4$ T, well exceeds the thermal energy, $k_B T\approx 5\ \mu\text{eV}$, at typical experimental temperatures ($T=70$ mK) with effective g factor $g^*=0.44$, Bohr magneton μ_B, and Boltzman constant k_B. In a first approximation, each LL in the QD's increases its energy as the boundary of the QD's is approached. At the energy position where a LL crosses the Fermi level, the level flattens due to screening effect of the electrons forming a compressible region, where the relevant electron states are partially occupied.[19,20] The spin-up and the spin-down lowest LL's (LL0↑ and LL0↓) thus yield, respectively, outer and inner ring-shaped metallic regions as schematically shown in Fig. 1(a). The partially occupied first LL (LL1↑) forms a compressible metallic core region.[18] These metallic regions are separated from one another by incompressible insulating stripes. For the sake of brevity, we will refer to LL0↑, LL0↓, and LL1↑, respectively, as levels 1, 2, and 3 below.

The conduction through the dot occurs via tunneling of electrons between the metallic outermost ring of the level 1 and reservoirs. In the SET operation, the conductance through the dot is nonzero only when the electrochemical potential of level 1, μ_1, lines up with the electrochemical potential of the reservoirs (the Fermi level E_F). The tunnel probability between the inner ring (core) of the level 2 (3) and the reservoirs is negligibly small. However, the numbers of electrons on these levels strongly affects the conduction through the dot because they influence μ_1 through capacitive coupling to the metallic region of the level 1. A similar system has been studied experimentally[18,21] and theoretically,[22] but detailed analysis was restricted to the two-level case with two lowest LL's ($\nu<2$). The underlying physics is analogous also to that of parallel QD's studied by Hofmann and co-workers.[23] Below we will expand the treatment of these authors to the three-level system with $2<\nu<3$.

We designate the electrostatic capacitances formed between the metallic regions of levels i and j as C_{ij} and that between the metallic region of level i and the outside surroundings as C_i, which are schematically shown in Fig. 1(b). When the gate bias voltage V_g and the magnetic field B are fixed, the number of electrons in each level (N_i, N_2, N_3) is determined so that the total energy of electrons in the dot, $E(N_1,N_2,N_3,V_g,B)$, is minimized. The electrochemical potential of each level, μ_i, is defined as a minimal energy necessary to add one electron to the level i while keeping the electron numbers on the other levels unchanged:

$$\mu_i(N_i,N_j,V_g,B)=E(N_i,N_j,V_g,B)-E(N_i-1,N_j,V_g,B), \tag{1}$$

where j refers to the other level ($j\neq i$). Below we will drop V_g and B from the notations for brevity of description although μ_i are always a function of V_g and B. The electrochemical potential for other configurations with $N_j+\Delta N_j$ electrons on the jth levels (j is one of three numbers 1, 2, and 3) can be written as

$$\begin{aligned}\mu_i(N_j+\Delta N_j)&=\mu_i(N_j)+\sum_j U_{ij}\Delta N_j\\ &=E_i-e\varphi_i+\sum_j U_{ij}\Delta N_j-\alpha_i eV_g,\end{aligned} \tag{2}$$

where E_i is the chemical potential term for the level i in the configuration of (N_1,N_2,N_3) (or the single-particle-state energy in the compressible metallic region of the level i), $e\varphi_i$ with the unit charge e is the electrostatic potential energy, and α_i is a positive coefficient less than unity, representing capacitive coupling between the control gate and metallic region i. The term $\sum_j U_{ij}\Delta N_j=e\Delta\varphi_i$ represents the electrostatic potential energy induced by the change $N_j\rightarrow N_j+\Delta N_j$ ($j=1$, 2, and 3), where we will refer to $[U_{ij}]$ as the charging energy matrix.

In the limit of an infinitely large two-dimensional electron gas (2DEG), the single-particle state energy E_i is independent of N_i, viz., $E_1=(1/2)\hbar\omega_c-g^*\mu_B B/2$, $E_2=(1/2)\hbar\omega_c$

$+g^*\mu_B B/2$, and $E_3=(3/2)\hbar\omega_c-g^*\mu_B B/2$, where $\omega_c=eB/m^*$ is the cyclotron angular frequency with the effective mass of the electron $m^*=0.068m_0$. Although the energy spacing, $\Delta E_i=E_i(N_i+1)-E_i(N_i)$, may be nonzero in real QD's, we suppose that $\Delta E_i \ll U_{ij}$, and ignore ΔE_i in the following analysis for the relatively large QD's.

As shown in the Appendix, the charging energy matrix can be approximately expressed as

$$[U_{ij}]\approx A\begin{pmatrix} 1 & 1-\dfrac{C_2}{C_{12}} & 1-\dfrac{C_2}{C_{12}}-\dfrac{C_3}{C_{23}} \\ 1-\dfrac{C_2}{C_{12}} & 1+\dfrac{C_1-C_2}{C_{12}} & 1+\dfrac{C_1-C_2}{C_{12}}-\dfrac{C_3}{C_{23}} \\ 1-\dfrac{C_2}{C_{12}}-\dfrac{C_3}{C_{23}} & 1+\dfrac{C_1-C_2}{C_{12}}-\dfrac{C_3}{C_{23}} & 1+\dfrac{C_1-C_2}{C_{12}}-\dfrac{C_3}{C_{23}}+\dfrac{C_1+C_2}{C_{23}} \end{pmatrix} \tag{3}$$

by leaving the lowest-order terms in C_i/C_{ij}, where we will refer to

$$A=U_{11}\approx\frac{e^2}{C_1+C_2+C_3} \tag{4}$$

as the charging energy of the QD. Here, we use the inequality relations

$$C_{12}\gg(C_1,C_2)\gg C_3 \quad\text{and}\quad C_{12}\gg C_{23}\gg C_{13}\gg C_3, \tag{5}$$

which generally hold for the present concentric geometry of relevant metallic regions.

Let us introduce an additional energy parameter

$$\begin{aligned}\Delta\varepsilon_{ij}(N_i,N_j)&=E(N_i-1,N_j+1)-E(N_i,N_j)\\&=-\Delta\varepsilon_{ji}(N_i-1,N_j+1)\\&=\mu_j(N_i-1,N_j+1)-\mu_i(N_i,N_j)\\&=\mu_j(N_i,N_j)-\mu_i(N_i,N_j)+U_{jj}-U_{ji},\end{aligned} \tag{6}$$

which represents the total energy change induced by the intradot transfer $i\rightarrow j$ of one electron.

For a given total number of electrons, a particular configuration (N_1,N_2,N_3) gives the ground state of the QD if the relations

$$0\leqslant\Delta\varepsilon_{ij}(N_1,N_2,N_3)<U_{jj}-U_{ji} \tag{7}$$

are satisfied for any set of levels (i and j). The energy $\Delta\varepsilon_{ij}$ increases by $\Delta\varepsilon_{ij}(N_i-1,N_j+1)-\Delta\varepsilon_{ij}(N_i,N_j)=U_{ii}+U_{jj}-2U_{ij}=e/C_{ij}$ after the transition $i\rightarrow j$ (where i and j two adjacent levels), but is kept unchanged after other transitions between another adjacent levels $l\rightarrow m$ because $\Delta\varepsilon_{ij}(N_l-1,N_m+1)-\Delta\varepsilon_{ij}(N_l,N_m)=0$ (one of two indexes l and m is different from i and j). We note that in the evolution of the ground state the transition $3\rightarrow1$ ($1\rightarrow3$) never occurs because $\Delta\varepsilon_{31}(N_1,N_2,N_3)=\Delta\varepsilon_{32}(N_1,N_2,N_3)+\Delta\varepsilon_{21}(N_1,N_2+1,N_3-1)=\Delta\varepsilon_{32}(N_1,N_2,N_3)+\Delta\varepsilon_{21}(N_1,N_2,N_3)\geqslant0$, as seen from Eqs. (3), (6), and (7).[24]

As V_g increases, μ_i for each level i decreases according to Eq. (2). One electron can be added on the level i when μ_i reaches E_F. Particularly, the conductance through the QD becomes nonzero when $\mu_1=E_F$. Appreciable conductance does not take place, if $\mu_2=E_F$ or $\mu_3=E_F$, however, because the tunnel coupling between the relevant levels and the reservoirs is too small in the experimental condition. It follows that the conductance peak position,

$$V_g=\left(E_1-e\varphi_1+\sum_j U_{1j}\Delta N_j-E_F\right)/(\alpha_1 e),$$

traces exclusively the μ_i for $i=1$. The charging energy, Eq. (4), represents an increment of μ_1 upon the addition of one electron to level 1 ($\Delta N_1=1,\Delta N_2=\Delta N_3=0$) and gives the conductance peak spacing, $U_{11}/(\alpha_1 e)$, in the sweep of V_g.

Suppose that the QD is in the ground state, (N_i,N_2,N_3), at given values of B and V_g. As B increases at the fixed V_g, each one-particle wave function is squeezed to increase the LL degeneracy. All the electrons in the dot are accordingly compressed towards the dot center, leading to an increase and a decrease of the electrostatic potential, respectively, in the interior region and in the boundary region of the dot. This, together with the B dependence of E_i, gradually decreases $\mu_1-\mu_2$ and $\mu_2-\mu_3$ as B increases. When B reaches a position at which $\Delta\varepsilon_{ij}(N_i,N_2,N_3)=0$, the ground-state configuration changes from (N_i,N_j) to (N_i-1,N_j+1). Equation (2) shows that such an electron transfer, $3\rightarrow2$ or $2\rightarrow1$, causes a shift of μ_1 by

$$\Delta\mu_1(ij)=U_{1j}-U_{1i}, \tag{8}$$

where $(ij)=(32)$ or (21), which results in the conductance peak jump towards the positive direction by

$$\Delta V_g(32)=(C_3/C_{23})U_{11}/(\alpha_1 e)$$

$$\text{or}\quad \Delta V_g(21)=(C_2/C_{12})U_{11}/(\alpha_1 e). \tag{9}$$

As it will be shown later, these amplitudes, $\Delta V_g(ij)$, are smaller than the fundamental conductance peak spacing by a factor $C_i/C_{ji}\approx0.02$–0.2, but sufficiently large to be experimentally discerned.

We assume that $\Delta\varepsilon_{32}$ and $\Delta\varepsilon_{21}$ decrease linearly with increasing B in a small interval of B as schematically shown in Fig. 2. As noted above, $\Delta\varepsilon_{ij}$ jumps by e^2/C_{ji} at the B position where $\Delta\varepsilon_{ij}$ reaches zero, but $\Delta\varepsilon_{32}$ and $\Delta\varepsilon_{21}$ do not interfere with each other.[25] Accordingly, they exhibit, respectively, simple toothlike behavior, spanning the ranges

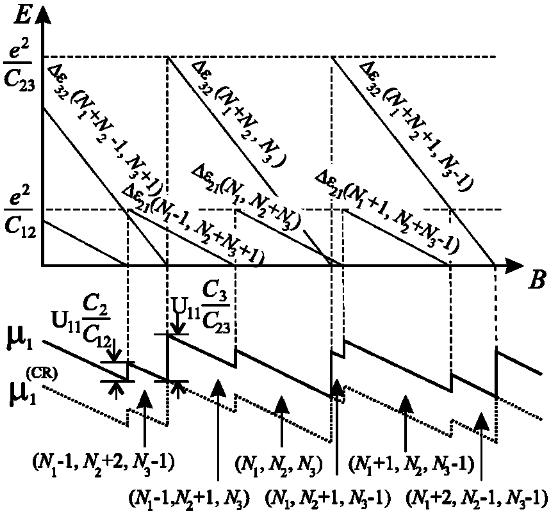

FIG. 2. The upper panel schematically shows excitation energies, $\Delta\epsilon_{23}$ and $\Delta\epsilon_{12}$, as a function of magnetic field. The lower panel shows the electrochemical potential μ_1 in the ground state (solid line) and the electrochemical potential $\mu_1^{(CR)}$ in the singly excited state (dashed line). As the magnetic field increases to the position at which $\Delta\epsilon_{23}=0$ $(\Delta\epsilon_{12}=0)$, the ground state changes its electron configuration through electron tunneling $3\rightarrow2$ $(2\rightarrow1)$. The tunneling event causes μ_1 as well as $\mu_1^{(CR)}$ to increase by $U_{11}C_3/C_{23}$ $(U_{11}C_2/C_{12})$.

$$0\leqslant\Delta\varepsilon_{32}\leqslant e^2/C_{23} \quad \text{and} \quad 0\leqslant\Delta\varepsilon_{21}\leqslant e^2/C_{12}. \tag{10}$$

These processes are accompanied by the variation of μ_1 followed from Eq. (8) as shown with a solid line in Fig. 2.

Let us consider effects of a cyclotron resonance (CR) excitation inside the dot.[26,27] Two different classes of transitions, LL0↑→LL1↑ and LL0↓→LL1↓, can occur as schematically shown in Fig. 3. In either process, the excited electron will rapidly give up its excess energy to the lattice, probably within several nanoseconds, and fall to the core region of LL1↑ (level 3).[28] The excited hole will similarly lose its energy and rapidly climb up to the ring region of either LL0↑ (level 1) or LL0↓ (level 2). As a result of this relaxation, the hole will eventually tunnel to the ring region of LL0↓ (level 2) because it is energetically more favorable for the hole to be on LL0↑ (level 1), as follows from inequalities $0<\Delta\varepsilon_{23}<\Delta\varepsilon_{13}$ derived from Eqs. (6) and (3) and relations (10).

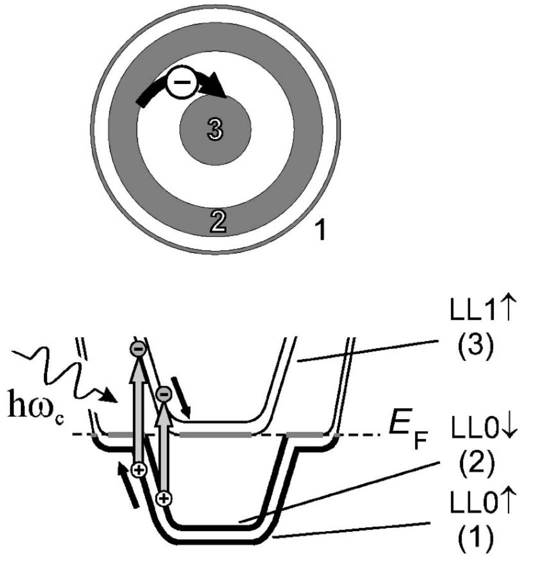

FIG. 3. In resonant photon absorption, an electron-hole pair is excited due to transition of either LL0↑→LL1↑ or LL0↓→LL1↓. The excited hole-electron pair is rapidly separated to polarize the QD.

We thus expect that the CR transition leads to the intradot electron transfer $2\rightarrow3$ after a relatively fast process of relaxation, which causes the conductance resonance peak to be discontinuously shifted by

$$\Delta V_g^{(CR)}=-(C_3/C_{23})U_{11}/(\alpha_1 e), \tag{11}$$

as derived from Eq. (8) with Eq. (3). This CR-induced shift is equal in amplitude but opposite in sign to the B-induced shift, $\Delta V_g(32)$, given in Eqs. (9), and is discernibly large in the experiments. As B is scanned, μ_1 in this relaxed excited state, $\mu_1^{(CR)}$, follows a trace similar to that of the ground state but shifted by $-(C_3/C_{23})U_{11}$, as is illustrated with a dotted line in Fig. 2.

Another important aspect is that the lifetime of the relaxed excited state can be extremely long because the excited electron-hole pair is well spatially separated. This makes the detection of a single-FIR-photon feasible. The total energy of the QD in the relaxed excited state, (N_1,N_2-1,N_3+1), is higher than that of the ground state, (N_1,N_2,N_3), by $\Delta\varepsilon_{23}^{(CR)}=\Delta\varepsilon_{23}$, which from Eqs. (6) satisfies the relation

$$\Delta\varepsilon_{23}^{(CR)}(N_1,N_2,N_3)=(e^2/C_{23})-\Delta\varepsilon_{32}(N_1,N_2,N_3). \tag{12}$$

As shown by Eq. (12) along with the behavior of $\Delta\varepsilon_{32}$ illustrated in Fig. 2, the energy $\Delta\varepsilon_{23}^{(CR)}$ increases until B reaches the transition position at which the ground-state configuration changes via an electron transfer $3\rightarrow2$: $\Delta\varepsilon_{23}^{(CR)}$ reaches a maximum value and drops to zero at the transition. This toothlike behavior of $\Delta\varepsilon_{23}^{(CR)}$ repeats as B increases further, while the amplitude of the tooth, e^2/C_{23}, increases with B because C_{23} decreases, as will be shown later. For instance, e^2/C_{23} increases from 0.2 meV at $B=3.4$ T to more than 2 meV at $B=4.0$ T. In typical conditions, $\Delta\varepsilon_{23}^{(CR)}$ is much larger than the thermal energy kT but substantially smaller than the cyclotron energy $\hbar\omega_c$ (6–7 meV).

III. EXPERIMENTAL SETUP

The studied QD's are fabricated by means of electron-beam lithography on a GaAs/Al$_x$Ga$_{1-x}$As heterostructure crystal. The sheet carrier density and the mobility of the 2DEG are $\mu=85$ m^2/V sec and $n_s=2.6\times10^{15}$ m^{-2}, respectively, at 4.2 K. A scanning electron micrography of a sample is shown in Fig. 4. Metal gates deposited on top of the heterostructure laterally define the QD, which is weakly coupled to the external 2DEG regions through tunnel barriers. The electrochemical potential of the QD, μ_1, is controlled by biasing the lower central gate. The metal gates along with the leads extend over about 100 μm length to form a dipole antenna that couples incident FIR radiation to the QD. An ac source-drain voltage, $V_{SD}=25$ μA, is applied at frequencies of 10 Hz–1 kHz, and conductance through the

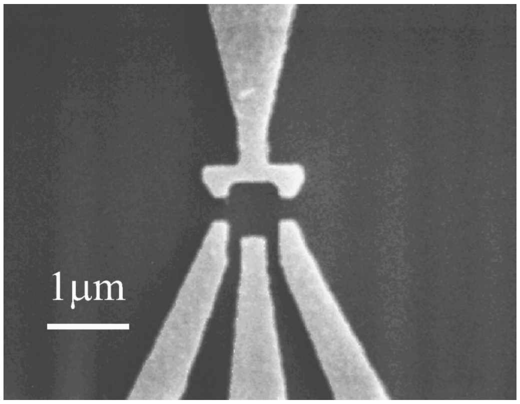

FIG. 4. Scanning electron microscope image of the QD.

QD is measured by a standard lock-in technique. The lithographic size of the dot is $0.7\times0.7\ \mu\mathrm{m}^2$, while the effective dot size, as it will be shown, is about $0.5\ \mu$m in diameter containing about 350 electrons. The charging energy of the QD, U_{11}, measured from I-V characteristics, is about [4×10^{-4} eV, which corresponds to $C_1+C_2+C_3=0.4fF$ as seen Eq. (4)]. We have studied three such QD's with nominally the same structure as described above. The QD is placed in a mixing chamber of a dilution refrigerator. Magnetic field B is applied normally to the plane of the QD with a superconducting solenoid.

A schematic view of the optical system is shown in Fig. 5. As a source of FIR radiation we use a 10-μm-wide 2DEG Hall bar ($\mu=20\ \mathrm{m}^2/\mathrm{V\,sec}$) fabricated on a GaAs/Al$_x$Ga$_{1-x}$As heterostructure crystal. When a current I_{emit} is passed through the Hall bar, the cyclotron resonance (CR) transition of nonequilibrium electrons yields cyclotron radiation at the frequency $\omega_c=eB/m^*$ ($m^*=0.068m_0$ with m_0 the free-electron mass).[29] An emission band is relatively narrow, being described by a Lorentzian curve with a full width at half maximum of about 10% around ω_c. The CR emitter is placed in the same mixing chamber at a distance of 27 mm from the QD sample. In additional experiments,[9] we installed CR emitters of a similar GaAs/Al$_x$Ga$_{1-x}$As 2DEG Hall bar as well as the n-type InSb device [$m^*=0.014m_0$) Ref. 30] in another superconducting solenoid placed outside the mixing chamber, at a distance of about 80 cm from the QD sample. The radiation is guided through a metal light pipe of 3 mm Ø bore to the QD. The wavelength of emitted FIR radiation was thus independently tuned over a range 0.1 mm$<\lambda<$2 mm by scanning the magnetic field, B_{emit}, for the emitters. The experiments show that FIR photons are detected only if the frequency coincides with the plasma-coupled CR frequency of the QD,[8,26,27]

$$\omega_{QD}=(\omega_c/2)+\{(\omega_c/2)^2+\omega_p^2\}^{1/2}, \tag{13}$$

where $\omega_p=17\ \mathrm{cm}^{-1}$ is the plasma frequency of the presently studied QD's. When the emitter is placed in the same mixing chamber as in the arrangement of Fig. 5, the relative position to the magnet center is adjusted so that the emitted radiation frequency approaches to ω_{QD}, which varies from $1.04\omega_c$ ($B=3.2$ T) to $1.01\omega_c$ ($B=4.2$ T).

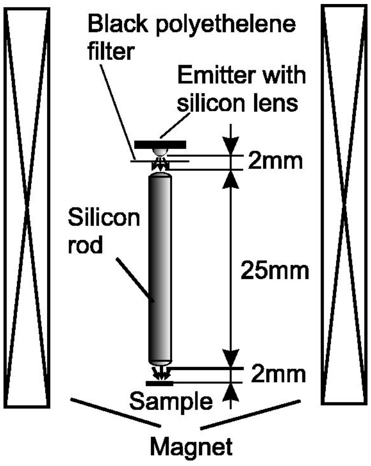

FIG. 5. Schematic representation of the experimental setup.

In either optical scheme, unwanted radiation in the near- and midinfrared regions is eliminated by filtering through pure silicon plates and black polyethylene films. We confirmed that continuous illumination of the QD for 24 hours did not lead to any appreciable change in the 2DEG density, indicating that not only the band gap light of GaAs but also longer wavelength lights that cause persistent photocurrents are completely eliminated. Single FIR photons are detected in a B range of 3.4–4.2 T, which corresponds to the wavelength range of $\lambda=220$–$170\ \mu$m.

The emitted FIR power from the source is very small, being roughly proportional to the square of I_{emit}. A radiation flux density incident in the vicinity of the QD is roughly estimated to be as low as $10^{-16}\ \mathrm{W/mm}^2$ for a bandwidth of $170\pm10\ \mu$m at $I_{emit}=3\ \mu$A (in the case when the emitter is placed inside the chamber), which implies about 10^3 incident photons per second on the effective antenna area of the QD (about 0.1 mm diameter).

IV. EXPERIMENTAL RESULTS

A. Transport in the ground state

Transport characteristics on three QD's have been studied in a magnetic field range of 3.2–4.5 T. The experimental results are similar among the three QD's. The conductance through the QD exhibits nearly equidistant sharp resonance peaks in the sweep of V_g as shown on one QD in the inset of Fig. 6(a) for $B=3.95$ T. The temperature of the mixing chamber is 70 mK, while an effective electron temperature in the QD is estimated to be 110 mK from the conductance resonance linewidth.[1] Figure 6(a) displays the peak positions of the conductance resonance as a function of B. A magnetic field position of $B\approx4.1$ T corresponds to $\nu=2$ in the QD as discussed below, which is reasonable compared to $B=5.6$ T where $\nu=2$ in the bulk 2DEG.

We find that in each trace the peak position fluctuates, yielding toothlike fine structures, where a superposition of two different series of steps is visible in the closeup given in Fig. 6(b): In one series, I, the steps are relatively large with a nearly unchanged height but the interval between them increases as B increases [seen in Fig. 6(a)]. The other series, II, consists of the steps that occur at a nearly constant B-interval while their heights are smaller in a lower B range but become larger with increasing B.[31] Any steps are of the direction towards positive voltages when B increases.

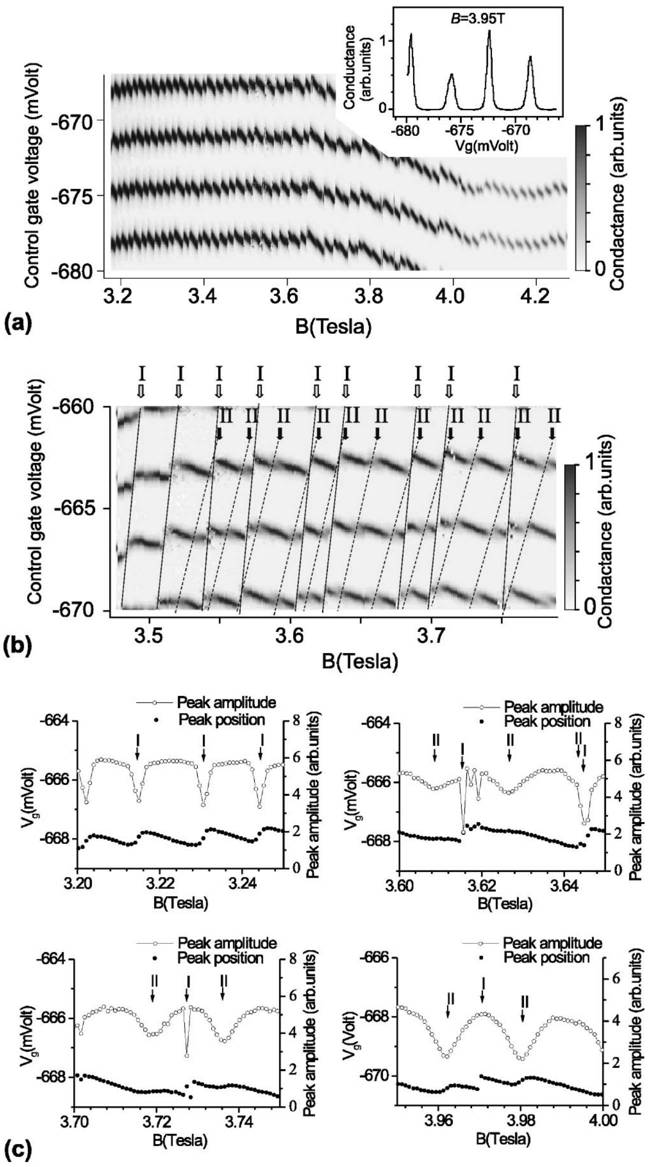

FIG. 6. (a) Conductance peak positions as a function of magnetic field. The inset shows an example of conductance oscillations at $B = 3.95$ T. (b) Enlargement of the conductance peak positions in a narrower range of magnetic field. (c) Amplitude and position of a conductance peak in different ranges of magnetic field.

The structure of series II is more clearly discerned by the downward cusp of the conductance peak amplitude as displayed in Figs. 6(c) together with the trace of the peak position for different intervals of B. Sharp cusps due to steps of series I are also visible. We find that every step occurs in such a way that one peak reduces its amplitude while another peak at a shifted V_g position grows to replace the former. The data shown in Figs. 6(c) are obtained by tracking a stronger peak.[32] As seen in Figs. 6(c), all these steps get sharper as B increases, while the steps of series I become so sharp that they are no longer traced in actual measurements at $B > 3.9$ T.

We find yet another feature: The B position of each step on one trace, either in series I or II, linearly shifts when going from one trace to another. Solid and broken lines are drawn in Fig. 6(b) to assist recognizing this systematic shift of the steps for series I and II, respectively.

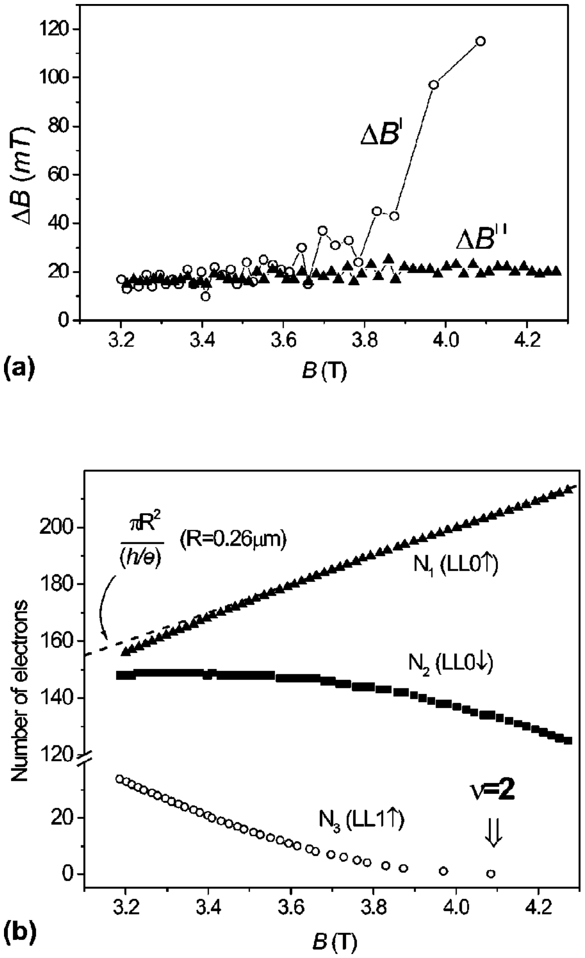

FIG. 7. (a) Intervals between successive steps of type I and II, ΔB^{I} and ΔB^{II}, against B. (b) Numbers of electrons in the different Landau levels against B.

We now discuss physical implication of these features. Figure 7(a) plots the step interval for both series. The interval in series I, ΔB^{I}, increases remarkably with increasing B until it diverges, the steps vanish, at $B \approx 4.1$ T, while that of series II, ΔB^{II}, is kept nearly unchanged ($\Delta B^{II} = 0.020$ T) in the entire B range.

We interpret the steps of series I and II as the structures arising, respectively, from one-electron transfers $3 \rightarrow 2$ and $2 \rightarrow 1$ discussed in Sec. II. Based on this interpretation, we can derive N_i in respective levels as a function of B. Noting that N_3 decreases by one at each step position of series I and that the step disappears ($N_3 = 0$) at $B > 4.1$ T, we find that $N_3 = 33$ at $B = 3.2$ T, and it decreases monotonically with increasing B until it vanishes at $B = 4.1$ T as plotted by open circles in Fig. 7(b). The relatively small number of electrons at $B = 3.2$ T, $N_3 = 33$, also indicates that the inner metallic core region (level 3) is substantially smaller than the dot size already at the lowest magnetic field. Noting that N_1 increases by one at each step of series II, we find that N_1 increases approximately linearly with B as plotted by the black triangles in Fig. 7(b). The linear increase of N_1 with B strongly suggests that the size of the outer metallic ring (LL0↑) is kept substantially unchanged over the entire studied B range and that N_1 increases by one each time when an extra magnetic flux quantum, $\Phi_0 = h/e$, is added to the outer metallic

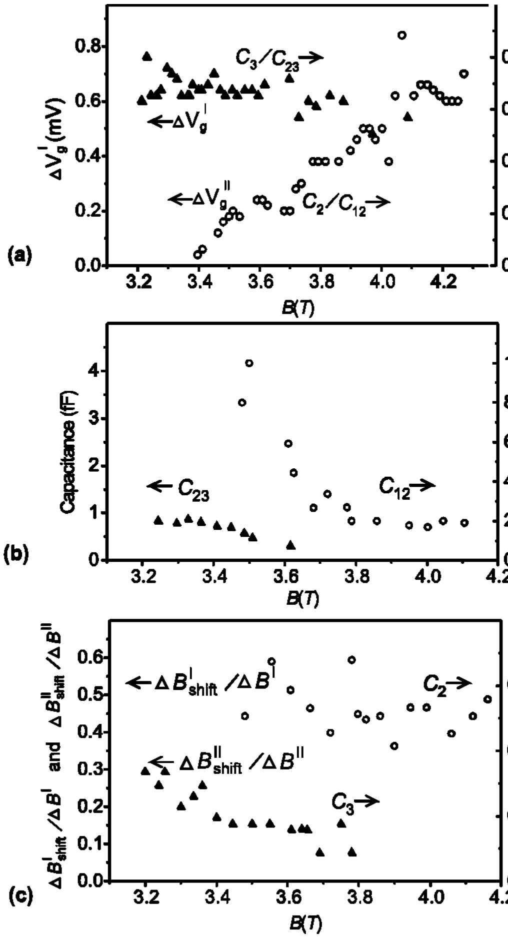

FIG. 8. (a) Heights of the steps of type I and II, ΔV_g^I and ΔV_g^{II}, against B. Capacitance ratios C_2/C_{12} and C_3/C_{23} are derived from ΔV_g^I and ΔV_g^{II}. (b) Values of C_{12} and C_{23} against B, derived from the analysis of conductance-peak amplitude. See text for details. (c) Shifts of step positions, ΔB^I_{shift} and ΔB^{II}_{shift}, between adjacent traces of the conductance peak normalized, respectively, by ΔB^I and ΔB^{II}_{shift}. Values of C_2 and C_3 are derived from $\Delta B^I/\Delta B^I$ and $\Delta B^{II}_{shift}/\Delta B^{II}$, respectively.

ring.[18] By assuming $N_1=0$ at $B=0$, we find that $N_1(B)$ is well fitted to the relation $N_1=\pi(D_1/2)^2B/\Phi_0$ as shown by the dotted line in Fig. 7(b), from which the diameter of the outer metallic ring, D_1, is derived to be 0.52 μm. We also find that $N_1=155$ electrons (with an uncertainty of ± 5 electrons) are accommodated in the lowest LL (LL0↑) at $B=3.2$ T. We can trace $N_2(B)$ by noting that it increases or decreases by one at each step of series I or II. We find that N_2 is kept nearly unchanged up to $B=3.6$ T, above which it starts decreasing substantially as plotted by black squares in Fig. 7(b). Hence, the inner metallic ring region (LL0↓) is suggested to start decreasing significantly with increasing B above 3.6 T. There is a larger ambiguity in the absolute number of N_2, but we assume $N_2=148\pm 15$ at $B=3.2$ T from the discussion below. Since the number of electrons, $N_1+N_2+N_3$, is fixed, the total spin is characterized by $N_2(B)$ in Fig. 7(b), which shows that the total spin starts to increase with B already before $\nu=2$ ($B=4.1$ T) is reached.

The interpretation in the above is supported by other characteristics of the step structures as discussed below. Figure 8(a) plots the height of steps, ΔV_g^I and ΔV_g^{II}, against B for series I and II. The step height ΔV_g^I does not change remarkably whereas ΔV_g^{II} significantly increases with increasing B as already mentioned. Values of C_3/C_{23} and C_2/C_{12} can be derived from the respective quantities through Eqs. (9), and indicated on the right-hand side vertical scale of Fig. 8(a). In Eqs. (9) we use $\alpha_1\approx 0.11$ and $U_{11}=4\times 10^{-4}$ eV ($C_1+C_2+C_3=0.4$ fF), determined from the spacing of conductance oscillations and the Coulomb staircase.[33] The ratio C_2/C_{12} is indiscernibly small in the small-B range below $B\approx 3.4$ T. This suggests that the inner metallic ring (level 2) is located closely to the outer ring (level 1), yielding much larger C_{12} than C_2, therefore, N_2 must be near N_1 at the lower B range. The significant increase of C_2/C_{12} in the higher B range suggests that the inner ring shrinks creating substantial separation to the outer ring. This behavior is consistent with the decrease of N_2 shown in Fig. 7(b). The ratio $C_3/C_{23}\approx 0.17$ does not change significantly with B. This can be understood by noting that both C_3 and C_{23} are roughly proportional to the size of the metallic core (level 3).

Let us consider the sharpness of the step structure [Figs. 6(c)]. As B approaches a critical position, B_c, for a transition $(N_i,N_j)\rightarrow(N_i-1,N_j+1)$ from the lower-B side, $\Delta\varepsilon_{ij}$ is reduced allowing thermal activation of the excited configuration. The conductance peak amplitude for the ground-state configuration will, therefore, be reduced as $P(N_i,N_j)=1/[1+\exp(-\Delta\varepsilon_{ij}/kT)]$, while the thermally excited-state conductance peak will grow as $P(N_i-1,N_i+1)=1/[1+\exp(\Delta\varepsilon_{ij}/kT)]$. Here, $\Delta\varepsilon_{ij}$ has been defined by Eq. (6), and $T=0.11$ K.[34] The transition of the conductance peak is hence sharper for larger $\Delta\varepsilon_{ij}$. Assuming a linear dependence of $\Delta\varepsilon_{ij}$ illustrated in Fig. 2 along with relations (10), we can write $\Delta\varepsilon_{32}(B)=\{(B-B_c^I)/\Delta B^I\}(e^2/C_{23})$ (for $B_c^I<B<B_c^I+\Delta B^I$) or $\Delta\varepsilon_{21}(B)=\{(B-B_c^{II})/\Delta B^{II}\}(e^2/C_{12})$ (for $B_c^{II}<B<B_c^{II}+\Delta B^{II}$), where values of ΔB^I and ΔB^{II} are indicated in Fig. 7(a). The observed B dependence of the peak amplitude shown in Fig. 6(c) is well reproduced by the curves of $P(N_i,N_j)$ and $P(N_i-1,N_i+1)$, from which values of C_{23} or C_{12} are derived as fitting parameters and plotted in Fig. 8(b).[35] The capacitance C_{12} is large in a lower B range but decreases significantly with increasing B in the range 3.4–3.7 T, being consistent with the behavior of the inner ring (level 2) described above. The capacitance C_{23} is substantially smaller than C_{12} in the entire B range and decreases further with increasing B until it becomes indiscernibly small at $B>3.8$ T. This feature reassures the vanishing of the metallic core region (level 3) at a higher B.

Combining the data of Figs. 8(a) and 8(b), one can immediately derive values of C_2 and C_3:C_3 is about 0.16 fF at $B=3.2$ T and decreases to an indiscernible level with increasing B above $B\sim 3.8$ T, suggesting again vanishing of the inner core: $C_2\sim 0.2$ fF does not change remarkably in the studied B range.

In order to cross-check our analysis, remember that the position of each step shifts when going from one trace to another. See the straight lines in Fig. 6(b). The shift between two traces normalized by the step interval, $\Delta B^I_{shift}/\Delta B^I$ or $\Delta B^{II}_{shift}/\Delta B^{II}$, is plotted in Fig. 8(c). The upper adjacent trace refers to an electron configuration containing one electron more on level 1. Therefore, the shift of steps when going to the adjacent trace comes from change in the excitation energy, $\Delta\varepsilon_{32}(N_1+1)-\Delta\varepsilon_{32}(N_1)=(C_3/C_{23})U_{11}$ or $\Delta\varepsilon_{21}(N_1+1)-\Delta\varepsilon_{21}(N_1)=(C_2/C_{12})U_{11}$. Hence, the ratios in the above are written as $\Delta B^I_{sift}/\Delta B^I=(C_3/C_{23})U_{11}/(e^2/C_{23})=C_3/(C_1+C_2+C_3)$ and $\Delta B^{II}_{shift}/\Delta B^{II}=(C_2/C_{12})U_{11}/(e^2/C_{12})=C_2/(C_1+C_2+C_3)$, from which the capacitance values of C_3 or C_2 are derived with $C_1+C_2+C_3\approx 0.4$ fF as indicated on the vertical scale of Fig. 8(c). These values of C_3 and C_2 are in fair agreement with those derived from Figs. 8(a) and 8(b), supporting the consistency of our analysis. Note here that C_2 is larger than 0.2 fF, which is more then 50% of $C_1+C_2+C_3$. This implies $C_2>C_1$, which infers that the outer ring (level 1) is a narrow strip and its effect of electrostatic shielding is small, this is consistent with the unchanged D_1 over the B range. The capacitance C_3 is distinctly smaller than C_2 and vanishes in a higher B range.

As a brief summary of this section, all the characteristic features of the conductance resonance peak indicate the following: (i) The outer metallic ring (level 1) consists of a narrow strip, and its effective diameter $D_1=0.52$ μm is substantially unchanged over the B range of 3.2T–4.2 T, (ii) the inner metallic ring (level 2) is close in size to the outer ring in a lower B range below 3.4 T but starts shrinking substantially with increasing B above 3.6 T, and (iii) the inner metallic core (level 3) is much smaller than the two rings already at $B=3.2$ T and further decreases its size until it disappears at about $B=4.1$ T. Most of the features of the transport through the QD have thus been derived by considering only the classical electrostatics. The picture is also consistent with theoretical calculations of QD's at high magnetic fields made by Stopa.[36]

For the later discussion, we note that the diameters of the inner metallic ring and the core, D_2 and D_3, are linked to N_2 and N_3, roughly as $N_2=\pi(D_2/2)^2B/\Phi_0$ and $N_3=\beta\pi(D_3/2)^2B/\Phi_0$, where β (<1) is a filling factor of the level 3, which we assume to be nearly independent on B. It follows that the spatial separation between the core and the inner ring, $\Delta X=(D_2-D_3)/2$, increases with B until the core vanishes.

B. Effects of FIR illumination: Single-photon detection

Transport studies on unequally populated electrons in edge and bulk states in large Hall bars have shown that the electrons tunnel between the highest occupied LL and the lower LL's is strongly suppressed.[37] This suppression is markedly pronounced as B increases, approaching to $\nu=2$, probably because of increasing spatial separation between the relevant levels. This leads us to speculate that when an electron-hole pair is excited through CR in a QD, its lifetime in the relaxed excited state can be particularly long in a relatively narrow B range below about $B=4.1$ T $(\nu=2)$. Single FIR photons have been indeed detected in the expected range, $B=3.4$–4.2 T, where the inner core is well separated form the inner ring of the dot. The effects are similar among the two studied QD's. Although experimental results are not presented here, spectroscopic measurements have further demonstrated[9] that the effects of FIR on the conductance as described below are induced by the (plasma-shifted) CR of the QD [Eq. (13)].

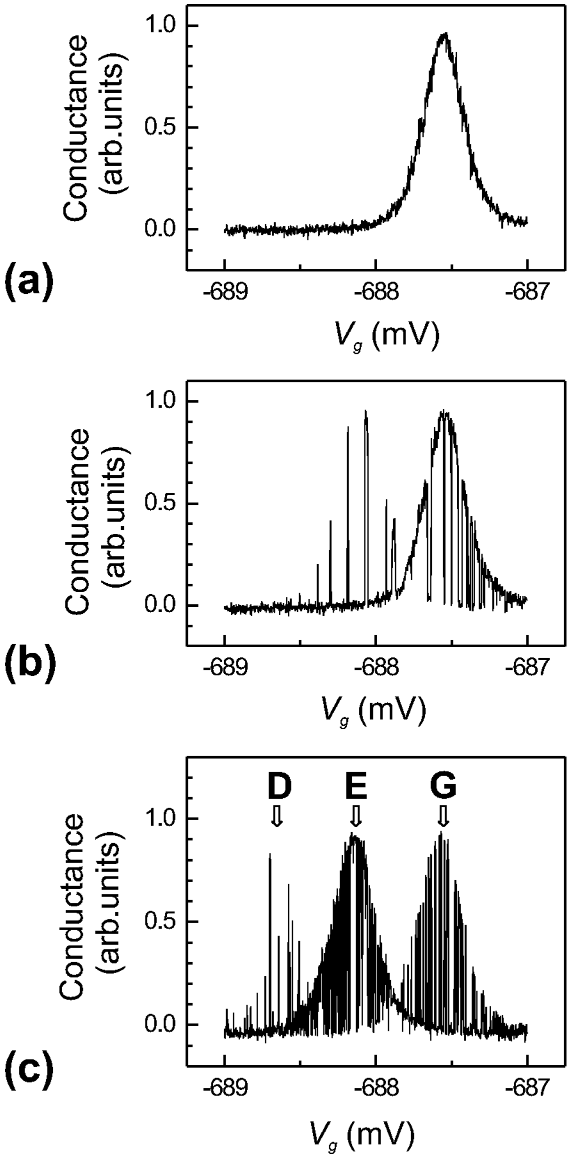

FIG. 9. Effects of FIR illumination on a conductance peak at $B=3.67$ T and $T=70$ mK. (a) Without FIR illumination. (b) Under extremely weak FIR illumination ($I_{em}=2$ mA). (c) Under less weak FIR illumination ($I_{em}=3.5$ mA).

Figure 9 displays a conductance peak in one of the investigated samples at $B=3.67$ T under different illumination intensities to exemplify the effect of FIR illumination. The time constant of measurements is 1 msec and the control gate voltage is scanned over 3 min for each curve. The original conductance resonance [Fig. 9(a)] is randomly switched off when very weak FIR illumination is turned on ($I_{em}=2$ μA) as shown in Fig. 9(b); at the same time, several spikes of finite conductance show up in a more negative V_g range. When the illumination is intensified ($I_{em}=3.5$ μA), the original conductance resonance, marked by G (ground state) in Fig. 9(c), can be identified as a series of conductance spikes, whilst conductance in the shifted V_g range grows to form a dense array of spikes defining a distinct envelope of another resonance peak, centered at the shifted position by $V_g=-0.55$ mV as marked by E (excited state). In addition, one can recognize that finite conductance also

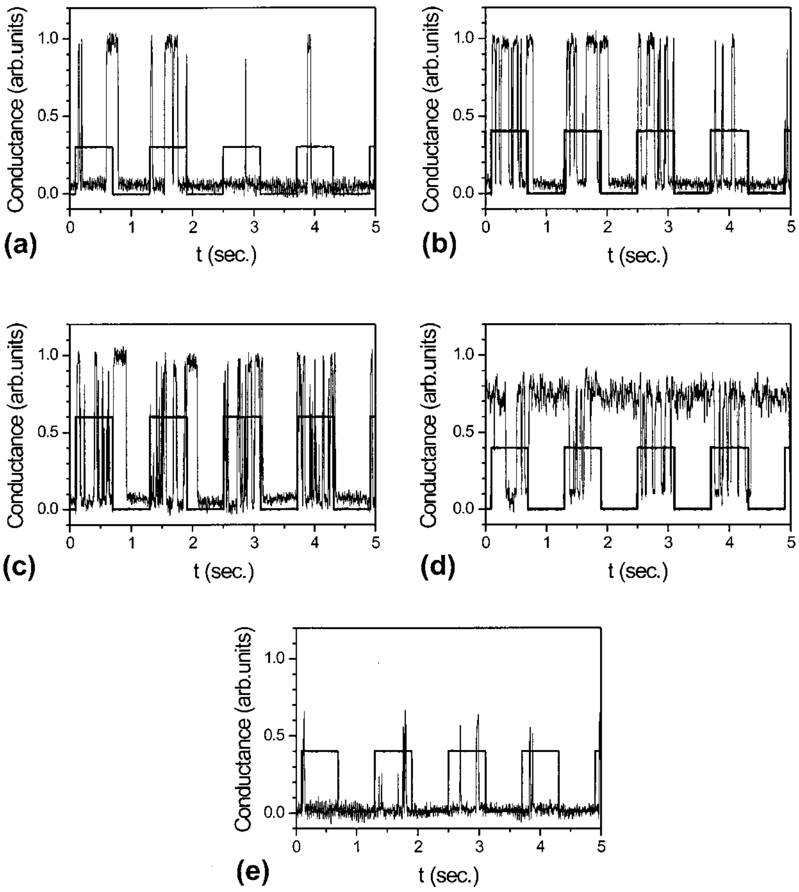

FIG. 10. Time traces of conductance under illumination of the form of square waves ($f \approx 0.8$ Hz). (a) $I_{emit}=1$ mA with V_g fixed at position E of Fig. 9(c). (b) $I_{emit}=2$ mA with the same V_g as in (a). (c) $I_{emit}=3$ mA with the same V_g as in (a). (d) $I_{emit}=2$ mA with V_g fixed at position G of Fig. 9(c). (e) $I_{emit}=2$ mA with V_g fixed at position D of Fig. 9(c).

takes place in the form of spikes in a V_g range shifted by $\Delta V_g=-1.1$ mV at $I_{em}=3.5$ μA marked as D (doubly excited state).

The shift, $\Delta V_g=-0.55$ mV, is equal in amplitude but opposite in sign to the one induced by the 3→2 transfer of an electron, ΔV_g^I in Fig. 8(a), as will be elucidated again in Fig. 13. This indicates that the new conductance resonance at position E arises from the 2→3 transfer of an electron as discussed at the end of Sec. II [Eq. (11)]. Furthermore, conductance resonance at the position D in Fig. 9(c) is interpreted as that due to the ‘‘doubly excited state’’ containing two electron-hole pairs within the QD.

When V_g is fixed at the position E for the resonance peak of the singly excited state, the conductance is normally switched off and is switched on each time when a single FIR photon is absorbed by the QD (G→E) as shown in Fig. 10(a), where the conductance at $B=3.6$ T is displayed as the time trace while the FIR radiation ($I_{em}=2$ μA) is modulated by square form current pulses of 0.8 Hz.

The dot is reset to the off-resonance state (E→G) when the excited electron-hole pair recombines. Figure 10(b) shows that the switching rate and the integrated time that the dot spends in the excited state increases with the FIR intensity ($I_{em}=3$ μA). Figure 10(c) shows, however, that at even higher level of excitation ($I_{em}=4$ μA) the integrated time spent in the excited state levels off, although the switching rate continues to increase. This is because the transition to the ‘‘doubly excited state’’ begins to play essential a role: If an additional electron-hole pair is excited before previously created electron-hole pair recombines, the QD undergoes transition to the doubly excited state (E→D), which switches off the conductance. This behavior will be elucidated more simply in Fig. 12(b).

Figure 10(d) demonstrates the telegraph signal obtained when V_g is set to the G position, for the original peak, with $I_{em}=3$ μA, where the conductance is normally gone: Each event of the switching-off corresponds to the transition G →E, and the switching-on corresponds to E→G. Here, the

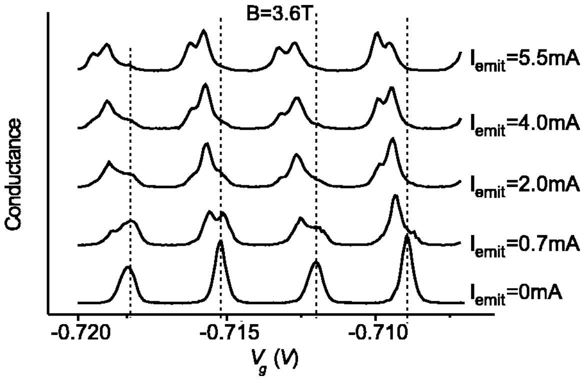

FIG. 11. Conductance oscillations taken over a long integration time ($\tau=300$ msec) under illumination up to a high intensity level. The maximal lifetime of the excited state in this sample at $B=3.60$ T is about 0.1 msec. It is a common feature that, with increasing illumination intensity (I_{emit}^2), the original conductance peak decreases its amplitude while a new peak corresponding to the singly excited state first grows at a position shifted towards the negative V_g direction and, at higher illumination intensities, yet another peak appears at the position shifted twice, corresponding to the doubly excited state. Dashed lines are guides for the eyes, marking the original peak positions.

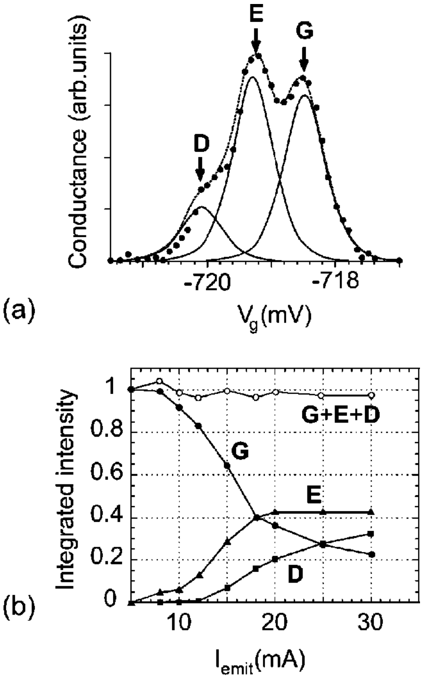

FIG. 12. (a) A time-averaged conductance peak at certain illumination intensity, data taken from Fig. 11. The experimental values (solid dots) are reproduced well by the dashed line showing is the superposition of three equally spaced peaks, G, E, and D (solid lines). (b) Variation of the amplitudes of the peaks, G, E, and D, against the illumination intensity ($\propto I_{emit}^2$), derived from the fitting procedure described in (a).

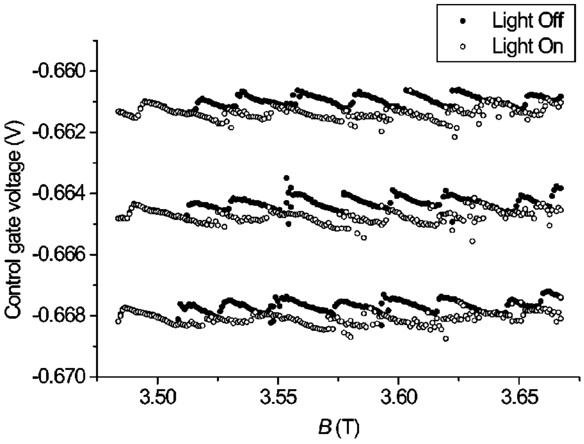

FIG. 13. Time-integrated positions of conductance peaks as a function of magnetic field without illumination (solid cycles) and under FIR illumination (open cycles). The illumination intensity is chosen so that peak E dominates. The amplitude of the peak shift due to the FIR illumination equals the step height, V_g^I, of the ground-state traces.

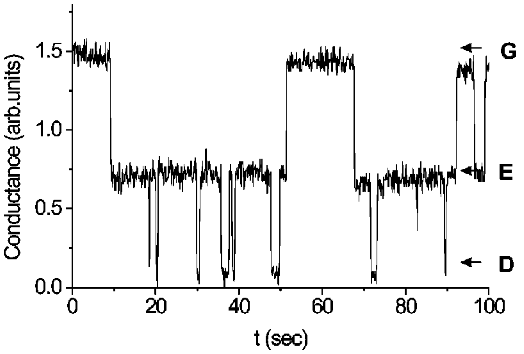

FIG. 14. Time trace of conductance at $T = 370$ mK ($B = 3.97$ T), where V_g is fixed at the ground-state peak position (G). Owing to the thermal broadening of the conductance peak, not only the switches of G↔E but also those of E↔D are visible.

transitions E→D or D→E are not visible because both of the singly excited and the doubly excited states yield the conductance ''off'' state when V_g is set to G. This is not the case when temperature is elevated, as will be shown later in Fig. 14. Figure 10(e) shows the data with V_g fixed at position D for the doubly excited state at $I_{em} = 3$ μA, where the events of switching-on and -off correspond, respectively, to the transitions E→D and D→E. We find that the lifetime of the doubly excited state (D) is much shorter than that of the singly excited state (E) so that of higher multiply excited states are not observable.

Similar effects as discussed above are found on every conductance peak in the B range of 3.4–4.2 T. Figure 11 displays a series of conductance peaks at $B = 3.6$ T averaged over a longer time constant of 300 msec for several different levels of FIR illumination. Individual conductance switches are not seen here because the time constant of measurements is much longer than the average lifetimes of excited states, which do not exceed 100 msec here. As the FIR is intensified for every conductance resonance, the original conductance peak at G reduces its amplitude while two additional conductance peaks develop at V_g positions, E and D, that are more negative.

The shape of conductance resonance line at any level of FIR excitation can be well reproduced by a superposition of the conductance peaks at V_g positions, G, E, and D, displaced to one another by about 0.55 mV. This is exemplified in Fig. 12(a), where the experimental values are indicated by black dots. The fitting procedure confirms that the V_g positions, G, E, and D, remain the same but the relative weight or the amplitudes of the resonance change with the excitation intensity. The amplitudes of the respective peaks represent the integrated intensities of the peaks and correspond to the integrated time, which the QD spends in the relevant states, or the switching rates multiplied by the lifetimes. Figure 12(b) displays the integrated intensity of respective peaks against I_{emit} (the FIR intensity $\propto I_{emit}^2$), and shows that the intensity of the singly excited peak at E first develops but levels off at a relatively strong excitation. The doubly excited peak at D becomes appreciable at a higher excitation level and continues to grow in the higher I_{emit} range where the singly excited peak is already saturated. The ground-state peak at G diminishes, while the total sum of the peak intensities, G+E+D, is kept unchanged in the entire I_{emit} range. This demonstrates that the QD is in one of the three states, G, E, and D and that other states do not contribute appreciable effects as already mentioned.[38] The features described in the above are the same for each conductance resonance line, reassuring our interpretation.

The V_g positions of conductance peaks under illumination ($I_{emit} = 3.5$ μA) are plotted as a function of B with open circles in Fig. 13, and compared with those obtained without illumination (solid circles). Here, the measurements are made again with an averaging time longer than the lifetime of the excited states, and the V_g positions of E are primarily traced. We note that the experimental points trace the expected plot of μ_1 shown in Fig. 2, providing compelling evidence that the conductance resonance (E) do indeed arise from the state containing one extra electron in the ''inner core.'' Several data points are located also at the doubly shifted positions ($\Delta V_g \approx -1.1$ mV), corresponding to the doubly excited state (D).

Figures 10(a) and 10(b) suggest that the recombination lifetime τ_L of an electron-hole pair in the relaxed excited state (E) of the dot is of the order of 100 msec in this condition of B and V_g. The lifetime is independent of the excitation level. We found that τ_L increases from the order of 1 msec at $B \sim 3.4$ T up to more than 100 sec at $B \sim 4.0$ T. The overall lifetime increase with B is roughly exponential, a similar behavior to the inverse of edge-bulk scattering rate in large quantum Hall bars.[37] We assume that the increase of τ_L correlates with the reduction in size of the inner core (level 3) of the QD. The maximum τ_L, being 1300 sec in one QD and 100 sec in another, is reached at a $B \approx 4.0$ T where only one electron remains in the inner core. When B exceeds this value, τ_L decreases, falling to a value of the order of 1 msec (at a B position ~ 4.2 T).

In addition to this overall behavior, τ_L discontinuously increases by 1 to 2 orders of magnitude at each position of B where an electron is transferred from level 3 (the inner core) to level 2 (the inner ring) in the ground state. This leads to a sharp and remarkable toothlike structure of τ_L, which correlates with the step structure of series I shown in Figs. 6(a) and 6(b).

We have confirmed that the conductance switches due to CR absorption within the QD is visible at elevated temperatures up to 400 mK. The effects of FIR excitation are similar to those at the base temperature ($T = 70$ mK) except that each line of conductance resonance becomes broader and that the lifetime of excited states is reduced roughly by one order of magnitude as temperature rises to 400 mK. Figure 14 displays a telegraphlike signal obtained by fixing V_g at position G of the original conductance peak when $T = 370$ mK. The magnetic field is set to be $B = 3.97$ T, at which the lifetime is maximal. Note that the singly and the doubly excited states at E and D are now distinguished in the conductance because of the thermal broadening.

V. DISCUSSION

The strikingly long lifetime τ_L of the relaxed excited state ($2 \rightarrow 3$) of the QD, observed under FIR illumination, indicates that the recombination rate of an excited electron in the inner core (level 3, LL1$\uparrow$) and a hole in the inner ring (level 2, LL0$\downarrow$) is extremely low. A very low recombination rate is reported also for an electron-hole pair excited in spin-resolved lowest LL's.[18] It has been theoretically suggested that the tunneling rate for QD's can be dramatically suppressed if the tunneling requires a complex rearrangement of all other electrons (in the inner core) due to many-body effects.[39] Let us speculate on whether such a particular mechanism is necessary or merely a spatial separation between the electron and the hole suffices for explanation the observed low tunnel rate.

We suppose that the tunnel transition takes place via an acoustical phonon emission. If the electron wave functions of the initial and the final states are separated, the squared matrix element for any tunnel transitions may be suppressed by the factor of an overlapping integral of the wave functions, which is approximated as $S = (\Delta X / l_B)^r \exp\{-(\Delta X / l_B)^2/2\}$, where $l_B = \{h/(e|B|)\}^{1/2}$ is the magnetic lengthened r is a constant taking a value of 2–3 depending on particular scattering mechanisms.[40] In the present case, $\Delta X \sim (D_2 - D_3)/2$ is the separation between the inner core and the inner ring, with D_3 and D_2 being, respectively, the diameter of the core (LL1$\uparrow$) and the internal diameter of the inner ring (LL0$\downarrow$). If we consider only the suppression factor S and assume analogy of inter-edge-state tunnel probability in wide Hall bars,[37,40] the value of τ_L and its dramatic overall increase with increasing B in the present experiments ($\tau_L \sim 1$ msec at 3.4 T and 100–1300 sec at 4.0 T) suggest that ΔX is about 80 nm at 3.4 T ($S \sim 10^{-11}$ with $l_B = 13.3$ nm) and increases to about 97 nm when B increases to 4.0 T($S = 10^{-11}$–10^{-12} with $l_B = 12.3$ nm). This behavior of ΔX, including its absolute size, appears to be reasonable in the present experimental condition and appears to be consistent with theoretical calculations, too.[36] We thus suggest that the observed extremely low tunneling rate can be explained only by considering the spatial separation. We, however, do not rule out the possibility that other mechanisms play an additional role in suppressing the tunnel rate.

As for the toothlike behavior of τ_L, we can mention qualitatively the following two relevant factors. First, ΔX does not increase smoothly with increasing B but increases stepwise at each transition position B_c^I of series I ($3 \rightarrow 2$). Second, when B increases, the excitation energy of the relaxed excited state, $\Delta \varepsilon_{23}^{(CR)}$, given in Eq. (12) increases with B until it drops from the maximum value e^2/C_{23} to zero at the transition position B_c^I. Therefore, the energy quantum released in the recombination process also increases with B up to e^2/C_{23} and then suddenly drops to zero at B_c^I.

For application of the described SET as a FIR-photon counter, it may be useful to discuss some features from the viewpoint of detector. First, although the wavelength range of single-photon detection in the present experiments is limited to 0.17–0.22 mm, it may be easily expanded. In the current experiments, it is determined by the magnetic field range ($3.4 - 4.15$ T) where τ_L exceeds the time constant of measurements (1 msec). The time constant is restricted by our present instrumental setup consisting of twisted-pair wiring along with a slow current amplifier operating at room temperature. The intrinsic limit on the SET speed of is greater than 10 GHz. In practice, implementation of a scheme of rf SET[41] is possible, which can improve the time resolution down to 10 nsec. The wavelength range can be also significantly expanded. An additional way to expand the range is to incorporate a back-gate structure into the QD, which facilitates control of the optimum B range.

Second, the stability of the SET in terms of dark counts is excellent: Very few conductance switches are seen in the absence of illumination. The ''dark current'' in terms of the switching rate is less than 0.001/sec at $T = 0.07$ K in a certain B range.

Third, the quantum yield β or the ratio of the photon count to the incident photon flux on the effective antenna area (0.1 mm diameter) is roughly estimated to be 1%, $\beta \approx 0.01$. The quantum yield, which crucially depends on the optics including an antenna structure, a QD geometry, and the substrate, may be further optimized.

Finally, we roughly compare the sensitivity of our QD detector with conventional FIR detectors. The highest sensitivity of conventional detectors reported in the literatures is of the order of 10^{-18} W/Hz$^{1/2}$ in terms of the noise equivalent power (NEP), which represents the power that can be detected with the signal-to-noise ratio of unity over 1 sec integration time. The sensitivity of our QD detector is limited by the rate of dark switches, which we roughly assume $\Delta t^{-1} = 0.001$ sec^{-1}. An effective value of the NEP may be derived from $\mathrm{NEP} = P/\Delta f^{1/2}$, where $P = \hbar\omega/(\beta\Delta t)$ (with photon energy $\hbar\omega$) is the ''noise'' power equivalent to the dark switching rate and $\Delta f = (2\pi\Delta t)^{-1}$ is the frequency band of measurement. Taking $\beta \approx 0.01$, $\Delta t = 1000$ sec, and $\hbar\omega \approx 6$ meV, we derive $\mathrm{NEP} = (2\pi)^{1/2}\hbar\omega/(\beta\Delta t^{1/2}) \approx 10^{-22}$ W/Hz$^{1/2}$. This value is superior to other conventional detectors by a factor more than 10^4.

VI. SUMMARY

Experiments have shown that different LL's in QD's at high magnetic fields ($2 < \nu < 3$) form regions of the inner core (LL1↑), the inner ring (LL0↓), and the outer ring (LL0↑) that are equivalent to electrically isolated metallic regions forming a capacitance network. The behavior of the conductance peak position with respect to the magnetic field has been analyzed successfully by considering the capacitance matrix.

Absorption of a FIR photon leads to addition of one extra electron to the core (LL1↑) and removal of an electron from the inner ring (LL0↓). The FIR-induced transfer of the electron yields an internal polarization of the QD that switches the conductance on or off through the QD. The lifetime of the excited state is long enough to be detected experimentally as individual conductance switches, realizing the single-FIR-photon detection. The lifetime has been found to increase with decreasing the size of the core region in the QD, reaching 20 min when just a few electrons remain in the core region.

ACKNOWLEDGMENTS

The work is supported by Core Research Evolutional Science and Technology (CREST) of Japan Science and Technology Corporation (JST). We thank M. Stopa for helpful discussion and calculations.

APPENDIX: CHARGING ENERGY MATRIX

Consider a capacitance network shown in Fig. 1(b). If the electrostatic potential in region i ($i = 1$, 2, or 3) changes by $\Delta\varphi_i$, the charge $e\Delta N_j$ induced on region j ($j = 1$, 2, or 3) is expressed as

$$e\begin{pmatrix} \Delta N_1 \\ \Delta N_2 \\ \Delta N_3 \end{pmatrix} = \begin{pmatrix} C_1 + C_{12} + C_{13} & -C_{12} & -C_{13} \\ -C_{12} & C_2 + C_{12} + C_{23} & -C_{23} \\ -C_{13} & -C_{23} & C_3 + C_{23} + C_{13} \end{pmatrix} \begin{pmatrix} \Delta\varphi_1 \\ \Delta\varphi_2 \\ \Delta\varphi_3 \end{pmatrix}, \tag{A1}$$

and the charging energy matrix $[U_{ij}]$,

$$e\Delta\varphi_i = \sum_j U_{ij}\Delta N_j, \tag{A2}$$

is the inverse of the capacitance matrix, and appears as the third term on the right-hand side of Eq. (2), viz., $[U_{ij}] = e^2[C_{ij}]^{-1}$.

In order to derive an approximate expression of $[U_{ij}]$, we note that in the present QD the largest ring-shaped region 1 surrounds the smaller ring-shaped region 2, which in turn surrounds the smallest core region 3 in the concentric geometry. In the B range studied here (3.3–4.2 T), the core region 3 contains at most only 10% of the total electrons and is substantially smaller than region 2 or 1. It follows that (i) the coupling between neighboring regions is much stronger than their couplings to the surroundings outside the QD, namely, $C_{12} \gg C_1$, C_2, and $C_{23} \gg C_2, C_3$; (ii) the 1-2 coupling is much stronger than the 2-3 coupling, and the 2-3 coupling is stronger than the 1-3 coupling, namely, $C_{12} \gg C_{23} > C_{13}$; (iii) the coupling of the region 3 to the surroundings outside the QD is much smaller than those of the regions 2 and 1 and is much smaller than the coupling to region 1, namely, $C_1, C_2 \gg C_3$ and $C_{13} \gg C_3$. These inequality relations are summarized in relations (5), from which Eq. (3) with Eq. (4) are derived.

---

*Present address: Department of Physics, Royal Holloway, University of London, Egham, Surrey TW20 0EX, England.

[1] L. L. Sohn, L. P. Kowenhoven, and G. Schön, *Mesoscopic Electron Transport*, edited by L. L. Sohn *et al.* (Kluwer Academic Publishers, Dordrecht, The Netherlands, 1997), pp. 105–214.

[2] M. Field, C. G. Smith, M. Pepper, K. M. Brown, E. H. Linfield, M. P. Grimshaw, D. A. Ritchie, and G. A. C. Jones, Phys. Rev. Lett. **77**, 350 (1996).

[3] J. M. Martinis and M. Nahum, Phys. Rev. B **48**, 18 316 (1993).

[4] L. P. Kouwenhoven, S. Jauhar, J. Orenstein, and P. L. McEuen, Phys. Rev. Lett. **79**, 2328 (1997).

[5] T. H. Ostercamp, T. Fujisawa, W. G. van der Wiel, K. Ishibashi, R. V. Hijman, S. Tarucha, and L. P. Kouwenhoven, Nature (London) **395**, 873 (1998).

[6] A. N. Cleland, D. Esteve, C. Urbina, and M. H. Devoret, Appl. Phys. Lett. **61**, 2820 (1992).

[7] R. J. Schoelkopf, S. H. Moseley, C. M. Stahle, P. Wahlgren, and P. Delsing, IEEE Trans. Appl. Supercond. **9**, 2935 (1999).

[8] D. Heitmann and J. P. Kotthaus, Phys. Today **46**, 56 (1993).

[9] S. Komiyama, O. Astafiev, V. Antonov, T. Kutsuwa, and H. Hi-

rai, Nature (London) **404**, 405 (2000).

[10] V. Antonov, O. Astafiev, T. Kutsuwa, H. Hirai, and S. Komiyama, Phys. E (to be published).

[11] C. de C. Chamon and X. G. Wen, Phys. Rev. B **49**, 8227 (1994).

[12] J. H. Oaknin, L. Martín-Moreno, J. J. Palacios, and C. Tejedor, Phys. Rev. Lett. **74**, 5120 (1995).

[13] A. Kalhede, S. A. Kivelson, K. Lejenell, and S. L. Sondhi, Phys. Rev. Lett. **77**, 2061 (1996).

[14] H. Imamura, P. A. Maksym, and H. Aoki, Proceedings of the 12th International Conference on EP2DS, Physica B **249-251**, 214 (1998).

[15] P. L. McEuen, E. B. Foxman, Jari Kinaret, U. Meirav, M. A. Kastner, Ned S. Wingreen, and S. J. Wind, Phys. Rev. Lett. **45**, 11 419 (1991).

[16] O. Klein, C. de C. Chamon, D. Tang, D. M. Abusch-Magder, U. Meirav, X.-G. Wen, M. A. Kastner, and S. J. Wind, Phys. Rev. Lett. **74**, 785 (1995).

[17] O. Klein, D. Goldhaber-Gordon, C. de C. Chamon, and M. A. Kastner, Phys. Rev. B **53**, 53 (1996).

[18] N. C. Van der Vaart, L. P. Kouwenhoven, M. P. de Ruyter van Steveninck, Y. V. Nazarov, C. J. P. M. Harmans, and C. T. Foxon, Phys. Rev. B **55**, 9746 (1997).

[19] D. B. Chklovskii, L. I. Glazman, and B. I. Shklovskii, Phys. Rev. B **46**, 4026 (1992).

[20] K. Bollweg, T. Kurth, D. Heitmann, V. Gudmundsson, E. Vasiliadou, P. Grambow, and K. Eberl, Phys. Rev. Lett. **76**, 2774 (1996).

[21] T. Heinzel, D. A. Wharam, J. P. Kotthaus, G. Boem, W. Klein, G. Trankle, and G. Weimann, Phys. Rev. B **50**, 15 113 (1994).

[22] A. K. Evans, L. I. Glatzman, and I. Shklovskii, Phys. Rev. B **48**, 11 120 (1993).

[23] F. Hofmann, T. Heinzel, D. A. Wharam, J. P. Kotthaus, G. Böhm, W. Klein, G. Tränkle, and G. Weimann, Phys. Rev. B **51**, 13 872 (1995).

[24] The transitions $3\rightarrow 2$ and $2\rightarrow 1$ can occur sequentially at certain positions of B and V_g where $\Delta\varepsilon_{32}=\Delta\varepsilon_{21}=0$.

[25] The independent behavior of $\Delta\varepsilon_{12}$ and $\Delta\varepsilon_{23}$ has simple physical meaning. As any two adjacent metallic regions are strongly capacitively coupled to each other ($C_i/C_{ij}\ll 1$), $\mu_i-\mu_j$ changes only when charge is redistributed between them (within C_{ij}), while charge redistribution outside the capacitance does not affect on the potential difference.

[26] P. A. Maksym and Tapash Chakraborty, Phys. Rev. Lett. **65**, 108 (1990).

[27] The excitation in the present experimental condition is that of center-of-mass motion as discussed in Ref. 26. Note that this excitation causes the inter-Landau-level transition.

[28] Spin-flip scattering is possible due to the spin-orbit interaction.

[29] Y. Kawano, Y. Hisanaga, and S. Komiyama, Phys. Rev. B **59**, 12 537 (1999).

[30] E. Gornik, M. Müller, and F. Gaderer, Infrared Phys. **16**, 109 (1976).

[31] In addition to the step structures, each trace smoothly moves towards the negative direction of V_g with increasing B up to 4.2 T. This overall shift is supposed to relate to the LL filling in the bulk 2DEG region outside the QD and will not be discussed in this paper.

[32] The peak position in Figs. 6(a) and 6(b) is represented by a weighted-average position of the double peaks in the vicinity of steps.

[33] α_1 and U_{11} are found to be nearly unchanged over the B range studied.

[34] We discuss here a feature averaged over a long time interval. Individual switching events between the two configurations can be resolved in time at some conditions as reported earlier by the group at Delft University (Ref. 17).

[35] For small steps, the analysis takes into account the resonance peak width as well.

[36] M. Stopa (private communication).

[37] S. Komiyama and H. Nii, Physica B **184**, 7 (1993).

[38] In still higher excitation levels, we find an appreciable contribution from the triply excited states with three electron-hole pairs excited in the dot.

[39] Y. V. Nazarov and A. V. Khaetskii, Phys. Rev. B **49**, 5077 (1994).

[40] S. Komiyama, H. Hirai, M. Ohsawa, Y. Matsuda, S. Sasa, and T. Fuji, Phys. Rev. B **45**, 11 085 (1992).

[41] R. J. Schoelkopf, P. Wahlgreen, A. A. Kozhevnikov, P. Delsing, and D. E. Prober, Science **280**, 1238 (1998).